

This article was published in an Elsevier journal. The attached copy is furnished to the author for non-commercial research and education use, including for instruction at the author's institution, sharing with colleagues and providing to institution administration.

Other uses, including reproduction and distribution, or selling or licensing copies, or posting to personal, institutional or third party websites are prohibited.

In most cases authors are permitted to post their version of the article (e.g. in Word or Tex form) to their personal website or institutional repository. Authors requiring further information regarding Elsevier's archiving and manuscript policies are encouraged to visit:

<http://www.elsevier.com/copyright>



Calibration of an HPGe detector and self-attenuation correction for ^{210}Pb : Verification by alpha spectrometry of ^{210}Po in environmental samples

Saïdou^{a,b}, François Bochud^a, Jean-Pascal Laedermann^a, Thierry Buchillier^a, Kwato Njock Moïse^b, Pascal Froidevaux^{a,*}

^aUniversity Institute of Radiation Physics, University of Lausanne, Grand-Pré 1, 1007 Lausanne, Switzerland

^bCentre for Atomic Molecular Physics and Quantum Optics, University of Douala, P.O. Box 8580 Douala, Cameroon

Received 3 April 2007; received in revised form 24 May 2007; accepted 5 June 2007

Available online 11 June 2007

Abstract

In this work the calibration of an HPGe detector for ^{210}Pb measurement is realised by a liquid standard source and the determination of this radionuclide in solid environmental samples by gamma spectrometry takes into account a correction factor for self-attenuation of its 46.5 keV line. Experimental, theoretical and Monte Carlo investigations are undertaken to evaluate self-attenuation for cylindrical sample geometry. To validate this correction factor, ^{210}Po (at equilibrium with ^{210}Pb) alpha spectrometry procedure using microwave acid digestion under pressure is developed and proposed. The different self-attenuation correction methods are in coherence, and corrected ^{210}Pb activities are in good agreement with the results of ^{210}Po . Finally, self-attenuation corrections are proposed for environmental solid samples whose density ranges between 0.8 and 1.4 g/cm³ and whose mass attenuation coefficient is around 0.4 cm²/g. © 2007 Elsevier B.V. All rights reserved.

PACS: 29.40.-n; 29.30.Kv; 23.60.+e

Keywords: HPGe calibration; ^{210}Pb ; ^{210}Po ; Self-attenuation correction; Environmental solid samples; Monte Carlo simulations

1. Introduction

Measurements of ^{210}Pb ($T_{1/2} = 22.3$ yr) have found numerous applications in the ^{210}Pb geochronometry of rapidly accumulating sediment environments and in studies of the behaviour of aerosols in the atmosphere [1]. Measuring its activity in air and in surface soils will provide quantitative information about the flux of ^{222}Rn and its daughters in the atmosphere [2]. Especially ^{210}Pb and ^{210}Po ($T_{1/2} = 138.4$ d) can be of great concern from the standpoint of radiation protection due to their radio-toxicity, as ^{210}Pb and ^{210}Po can accumulate in some foods and contribute significantly to the dose from total internal irradiation by ingested natural radionuclides [3,4]. Usually,

efficiency calibration for ^{210}Pb measurement by gamma spectrometry is realised by using a standard liquid solution of ^{210}Pb . If the source used for the efficiency calibration and the source under study differ with respect to their photon-attenuation properties, a correction should be applied [5].

^{210}Pb determination by gamma spectrometry in environmental solid samples is only possible through 46.5 keV photons. This low energy requires one to apply a self-attenuation factor to take into account the difference in composition of the sample with regard to the calibration standard solution [1]. In this work we use experimental, theoretical and Monte Carlo methods to determine the self-attenuation correction for the environmental solid samples in the cylindrical geometry [2,6]. The chemical composition of each analysed sample is determined by X-ray fluorescence and the experimental self-attenuation correction is

*Corresponding author. Tel.: +41 21 623 3480; Fax: +41 21 623 3435.
E-mail address: pascal.froidevaux@chuv.ch (P. Froidevaux).

based on the method proposed by San Miguel et al. [6] while theoretical and Monte Carlo approaches [2] are used for checking for coherence with the experimental method.

Assuming that ^{210}Po is at secular equilibrium with ^{210}Pb , alpha spectrometry performed on ^{210}Po can be used to independently estimate the activity of ^{210}Pb . Accordingly, the samples were processed by microwave acid digestion under pressure [7–9] and radiochemical separation in order to isolate ^{210}Po . Results of the same samples previously measured for ^{210}Pb are used to verify the self-attenuation correction methods. Finally self-attenuation corrections are proposed for environmental solid samples whose density ranges between 0.8 and 1.4 g/cm³ and whose mass attenuation coefficient is around 0.4 cm²/g.

2. Materials and methods

2.1. Sampling

In all, 20 soil samples from suspected uraneous areas of North Cameroon [10,11] were collected, dried, sieved, homogenised and kept for two years to assure equilibrium between ^{210}Pb and its daughter ^{210}Po .

2.2. Activity measurements

All measurements for ^{210}Pb were performed with a Canberra p-type HPGe well detector (GCW4523) with total active volume of 206 cm³, a relative photopeak efficiency of 45% and resolutions at 122 and 1332 keV of 1.24 and 1.93 keV, respectively. The simplified experimental set-up (detector–source geometry) is illustrated in Fig. 1. The associated electronics consisted of a Canberra preamplifier model (2002CSL) and an Accuspec[®] acquisition device. Treatment of the data was carried out with the GENIE 2000 program.

For ^{210}Po measurements, sources prepared by spontaneous deposition on silver discs were counted for alpha particles with Passivated Implanted Planar Silicon (PIPS)

detectors of 450 mm² active area in a Canberra Alpha Analyst spectrometer. The source–detector distance was 5 mm for all measurements allowing an efficiency of 25%. Standard sources of ^{241}Am and ^{239}Pu were used for the energy and efficiency calibrations of the detectors.

2.3. Chemical composition

The chemical composition of all the samples analysed in this study was determined at the Mineral Analysis Centre (CAM) of the University of Lausanne. After drying, sieving and calcinating at 1050 °C, 1.2 g of ash sample was mixed with 6 g of Li₂B₄O₇ and placed in a platinum crucible. The mixture was melted at 1150 °C to form a fused pastille. Finally, major elements of the sample were determined by X-rays fluorescence (Philips PW2400). The detection limit for major and trace elements was 0.01% and 1–5 ppm, respectively.

3. Self-attenuation correction

3.1. Experimental

The method consists in determining the full-energy peak efficiency of the calibration sample and of the analysed sample in the function of the sample height in the cylindrical geometry, a Semadeni 500 ml container (∅ = 9.5 cm, height = 8 cm) [6,12]. The calibration sample was a certified liquid solution of ^{210}Pb obtained from the Czech Metrological Institute, and the analysed sample for self-attenuation correction was a reference material (sediment) provided by the French Institut de Radioprotection et de Sûreté Nucléaire (IRSN) with reference activity values obtained through the IRSN 77 SR 300 interlaboratories comparison [13]. For each type of sample, the full-energy peak efficiency was determined at sample heights ranging from 1 to 8 cm. We plotted the different values of efficiency and the curve obtained could be approximated by a polynomial function of sample height as illustrated in Fig. 2. Efficiency calibration of the HPGe detector is then computed by fitting to the measurements the following empirical equation (6):

$$\varepsilon(h) = a_0 + a_1h + a_2h^2 \tag{1}$$

where h is the sample height (cm) and a_0, a_1, a_2 are the fitting parameters.

The self-attenuation factor of the sediment sample is then the ratio of the efficiencies computed with the sediment (ε_s) and with the calibration liquid solution (ε_r) given by the following empirical equation:

$$f_{\text{ex}}(h) = \frac{\varepsilon_s}{\varepsilon_r} = \frac{a_0 + a_1h + a_2h^2}{b_0 + b_1h + b_2h^2} \tag{2}$$

All uncertainty calculations on $f_{\text{ex}}(h)$ are presented in Appendix.

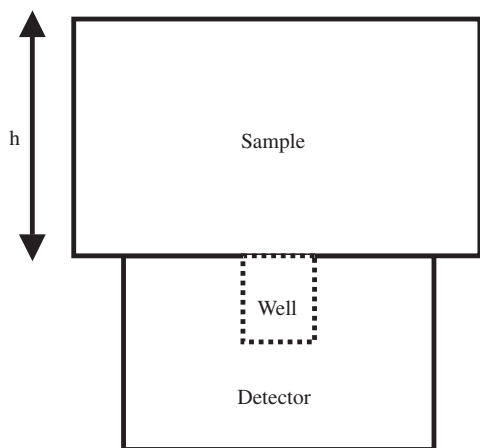


Fig. 1. Simplified schema of the experimental set-up (detector + source) where the sample container is posed on the endcap of the detector.

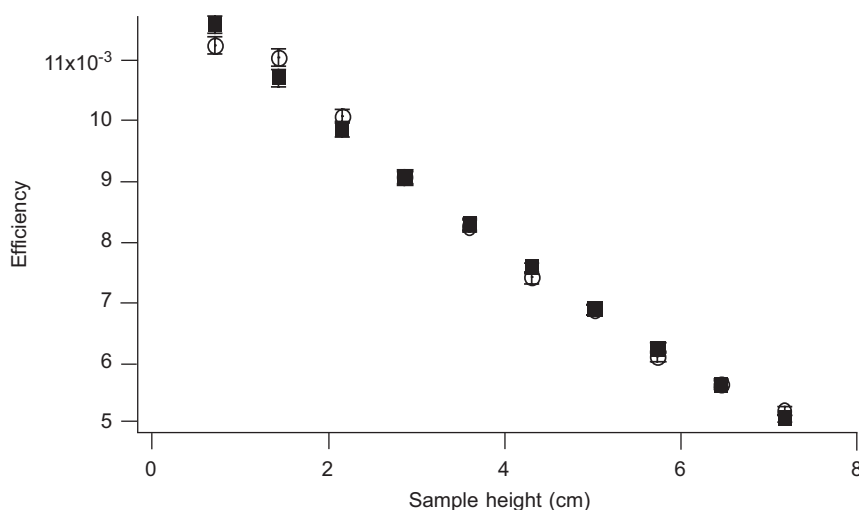


Fig. 2. Efficiency calibration of the HPGe detector against the sample height. The circle and black square, respectively, represent experimental and fitted efficiencies. The difficulty in distinguishing them proves that polynomial function is a good approximation of the experimental data.

3.2. Theoretical

Assuming that we have a plane source of thickness h with a homogeneous distribution of the attenuating material and activity, and that the trajectories of all photons originally starting into the solid angle subtended by the detector are normal to the source surface, the number n of photons finally emitted into this solid angle is [5]:

$$n = n_0 \left(\frac{1 - e^{-\mu\rho h}}{\mu\rho h} \right), \quad (3)$$

where n_0 is the number of photons produced within the sample which could reach the HPGe detector without self-absorption, ρ is the apparent density (g/cm^3) and μ is the mass attenuation coefficient (cm^2/g).

Because the total absorption efficiency depends directly on the number of photons impinging on the detector with a given energy, it can be expressed as:

$$\varepsilon = \varepsilon_0 \left(\frac{1 - e^{-\mu\rho h}}{\mu\rho h} \right), \quad (4)$$

where ε_0 is the full-energy peak efficiency in the absence of self-attenuation.

Thus the self-attenuation factor of the analysed sample is given by

$$f_{\text{th}}(h) = \frac{\varepsilon_s}{\varepsilon_r} = \left(\frac{\mu_r \rho_r}{\mu_s \rho_s} \right) \left(\frac{1 - e^{-\mu_s \rho_s h}}{1 - e^{-\mu_r \rho_r h}} \right), \quad (5)$$

and $\mu_{r,s} = \sum \omega_i \mu_i$ where ω_i and μ_i are, respectively, the mass fraction and the mass attenuation coefficient of each i element present in the sample.

The model described above yields accurate results if the sample height/sample diameter ratio is small and if the sample-detector distance is sufficiently large (typically several centimetres), so that scattered photons escape the detection solid angle. If this is not the case, the coherence

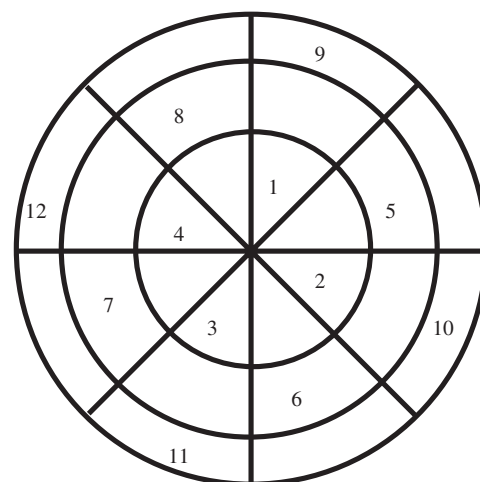


Fig. 3. Mosaic pattern of an air-filter standard. The individual sections are equal areas and do not touch each other. The mosaic allows the preparation of a pseudo-uniformly deposited source with no significant migration of the activity.

between experimental and theoretical results can be improved by taking into account the efficiency decrease due to sample-to-detector distance. The experimental settings consisted in depositing a known activity (^{210}Pb) on a filter of the same diameter as in the cylindrical geometry following the mosaic pattern of the International Electrotechnical Commission (IEC) [14]. To prepare the filter standard, filter paper of the same diameter as the sample container (Fig. 1) was divided into four sectors of equal area. Then the filter was divided again into three rings of equal area to have 24 equal-size areas as illustrated in Fig. 3. The mosaic pattern was transferred onto a translucent sheet of paper. Half of the filter was cut into its individual equal areas and each individual piece was placed onto the adhesive side of the tape. Finally, equal-size amounts of a standard solution of ^{210}Pb was put onto each

piece by a picnometer so that the total mass of the deposited solution is accurately known. The deposited solution was kept to air-dry overnight and the dried filter was covered with a piece of adhesive plastic so that the radioactivity is totally contained. The efficiency of the filter was then measured for several sample-to-detector endcap distances (x_i) and the results were fitted to the following empirical relation:

$$\varepsilon(x) = \varepsilon_0 e^{-\lambda x} \quad (6)$$

where ε_0 is the efficiency when the filter is on the detector end cap and λ (cm^{-1}) is the parameter to be determined with an exponential fit expression, which gives rise to an additional attenuation term in Eq. (5), namely

$$f_{\text{th}}(h) = \left(\frac{\lambda + \mu_r \rho_r}{\lambda + \mu_s \rho_s} \right) \left(\frac{1 - e^{-(\lambda + \mu_s \rho_s)h}}{1 - e^{-(\lambda + \mu_r \rho_r)h}} \right). \quad (7)$$

3.3. Monte Carlo

The GEANT 3.21 code, developed by CERN [15] was used for determining the self-attenuation factor by Monte Carlo calculation. This code was first designed for high-energy physics and it takes into account a large panel of particles. In particular, photons, electrons and positrons, as well as secondary electrons, are treated as long as their energy is above a cut-off of 10 keV. Below this threshold, the particles are stopped and their energy is considered as locally deposited. Previous studies performed by the authors with electrons and photons in an energy range between 10 and 3 MeV involved simulations, and experimental results have been used as a code validation for the present work [16,17,19,20]. The entire stochastic emission process, beginning with the decay scheme of the ^{210}Pb , was modelled using an internal code named Sch2for [17]. The particles emitted are simulated taking into account the geometry and composition of the sample itself and the detector. A space full of air at standard pressure filled the whole volume around the measuring facility.

Generally, each run involved the emission of 10^6 photons. Whenever a photon was generated, its history was followed until all its energy was dissipated in the sensitive volume of the detector. Such an event contributes to the full-energy peak and the corresponding efficiency is expressed by the ratio of the number of detected photons in the full-energy peak to the number of emitted photons. The self-attenuation factor was computed by the ratio between peak efficiencies of the measured solid sample and the liquid standard sample. Efficiency depends on the intrinsic characteristics of the detector, geometrical set-up and physico-chemical properties of the matrix [18]. In this work for every sample composition and height, the self-attenuation factor was determined.

Accurate knowledge of the detector geometry is important for efficiency uncertainty estimation, and recently Bochud et al. [19] showed that the Monte Carlo code used in the present study typically gave absolute computed

values that lie under 6% from the experimental efficiency data, depending on the uncertainties associated with the values of the detector parameters supplied by the manufacturer and/or incomplete charge collection in the crystal. However, because the self-absorption efficiency computed in this work implies relative quantities that may have large correlations, the associated uncertainties should be significantly lower.

4. Alpha spectrometry ^{210}Po measurement

4.1. Procedure

A procedure for ^{210}Po alpha spectrometry determination using microwave digestion under pressure for polonium solubilisation was developed. The method combines procedures from Refs. [7–9,21]. Briefly 30 ml of concentrated HNO_3 and 1 ml of ^{209}Po tracer were added to 1 g of solid samples (soil, sediment, etc.). Samples were heated in the microwave oven (Milestone MLS Ultra Clave) at 170°C for 40 min at a loading pressure of 60 bar. After filtration and dry evaporation at $80\text{--}90^\circ\text{C}$, being cautious to avoid temperatures above 100°C to minimise losses of polonium by volatilisation, the residue was dissolved in 40 ml of 2 M HCl. Two stacked cartridges containing Sr. Spec resin of Eichrom[®] (2 ml each) were conditioned with 10 ml of 2 M HCl and the sample solution was loaded on them by using a peristaltic pump. The cartridges were washed with 10 ml 2 M HCl, and interfering iron was eluted with 6 ml of 6 M HNO_3 . Finally polonium isotopes were eluted by 30 ml of 6 M HNO_3 and the solution was evaporated to dryness at $80\text{--}90^\circ\text{C}$. The residue was dissolved in 20 ml of 10^{-2} M HCl solution and was transferred to the deposition cell containing a silver disc of 1.7 cm in diameter. Mechanical stirring was used to facilitate polonium deposition. Time for quantitative deposition of polonium at ambient temperature was one day. After deposition, the disc was rinsed with distilled H_2O and acetone and dried at room temperature, then measured by alpha spectrometry. Overall yields were around 80%. To regenerate used cartridges, 30 ml of 0.5 M EDTA and 30 ml of distilled H_2O were passed through it. The above procedure is also valid for foodstuffs, whose quantity of dry sample to analyse was fixed to 5 g because of the detection limit of alpha spectrometry, which is 0.7 mBq for a counting time of one day.

4.2. Quality assurance

Quality assurance for the ^{210}Po determination developed in this work was performed using the IRSN reference material 77 SR 300 and IAEA reference materials IAEA-300 and IAEA-368. It led to the following results: IRSN 77 SR 300, ^{210}Po (−12.9%); IAEA-300, ^{210}Po (−17%); IAEA-368, ^{210}Pb (+16%). It should be noted that ^{210}Pb and ^{210}Po are considered to be at equilibrium.

5. Results and discussion

Experimental, theoretical and Monte Carlo self-attenuation factors were calculated for 15 sample heights ranging between 1 and 8 cm. Those for the IRSN reference solid sample are listed in Table 1. A simple test can be performed to check the agreement between two given data distributions. It should be noted that if the Z -scores were normally distributed, then the sum of the squared Z -scores should be χ^2 distributed [22]. For instance this can be translated into the following null hypothesis:

H_0 : There is no difference between experimental and theoretical self-attenuation corrections. $(Z_i)_{i=1,\dots,n}$ follows a normal distribution centred and reduced. n is the number of degrees of freedom corresponding to the number of sample heights. The probability to make a type-I error is $\alpha = 5\%$.

If H_0 is rejected then experimental and theoretical self-attenuation corrections are significantly different ($\alpha = 5\%$), otherwise we consider that the two corrections are not statistically different.

Comparison between theoretical and Monte Carlo self-attenuation factors shows that all Z values are negative. This could be justified by the fact that in the case of theoretical self-attenuation correction, we assumed that the trajectories of all photons originally starting into the solid angle subtended by the detector are normal to the source surface. This hypothesis underestimates the effective number of photons that are actually absorbed in the sample due to the underestimation of paths of certain photons whose trajectories are not normal to the source surface. This leads to the decrease of the probability of absorption of photons in the sample. By contrast, Monte Carlo simulation takes into account all types of emitted photon trajectories.

Table 2 lists the results of the χ^2 test on the Z -score values to test the H_0 hypothesis of the pairwise comparisons of the three methods. It appears that experimental, theoretical and Monte Carlo self-attenuation corrections are coherent with each other.

For ^{210}Pb activity measurements, after using the IRSN reference material for self-attenuation determination, 20 soil samples were measured by the HPGe detector, and their activities were estimated by the Genie 2000 software without self-attenuation correction. We applied to 20 soil sample activities the experimental self-attenuation correction found in the case of the IRSN reference material for our routine geometry corresponding to $h = 8$ cm. Monte Carlo self-attenuation correction, specifically computed for each sample composition, was also applied to the same soil sample activities obtained from Genie 2000 software.

Table 3 presents ^{210}Po activities (alpha spectrometry), ^{210}Pb activities (gamma spectrometry) corrected by experimental self-attenuation factor (IRSN reference material), and ^{210}Pb activities corrected by Monte Carlo self-attenuation factors. Table 3 also presents Z values between ^{210}Pb corrected activities and ^{210}Po activities for different soil samples. All Z values are within the interval of $|Z| = 2$. Although for experimental and Monte Carlo corrected activities their Z values are all negative, Table 4 shows how

Table 2
Statistical comparison based on the χ^2 test between experimental, theoretical and Monte Carlo self-attenuation factors ($\alpha = 5\%$)

Self-attenuation factor	n	χ^2	P (%)	H_0 rejected
f_{ex} / f_{th}	15	5.8	98.2	no
f_{ex} / f_{mc}	15	12.6	63.1	no
f_{th} / f_{mc}	15	4.1	99.7	no

n is the number of analysed sample heights.

Table 1
 Z score test results for experimental, theoretical and Monte Carlo self-attenuation corrections depending on sample height (cm)

Height (cm)	f_{ex}^{a}	f_{th}^{b}	f_{mc}^{c}	$Z_i (f_{\text{ex}}/f_{\text{th}})$	$Z_i (f_{\text{ex}}/f_{\text{mc}})$	$Z_i (f_{\text{th}}/f_{\text{mc}})$
1	1.048 ± 0.110	0.937 ± 0.033	0.960 ± 0.038	0.97	0.76	-0.60
1.5	0.998 ± 0.100	0.907 ± 0.045	0.929 ± 0.037	0.83	0.65	-0.59
2	0.949 ± 0.092	0.882 ± 0.056	0.898 ± 0.036	0.62	0.52	-0.44
2.5	0.901 ± 0.086	0.859 ± 0.064	0.876 ± 0.035	0.39	0.27	-0.48
3	0.855 ± 0.081	0.840 ± 0.071	0.856 ± 0.034	0.14	-0.01	-0.46
3.5	0.811 ± 0.077	0.823 ± 0.077	0.839 ± 0.033	-0.11	-0.33	-0.47
4	0.771 ± 0.075	0.809 ± 0.082	0.827 ± 0.033	-0.34	-0.68	-0.53
4.5	0.735 ± 0.074	0.796 ± 0.085	0.814 ± 0.032	-0.54	-0.98	-0.54
5	0.705 ± 0.072	0.786 ± 0.088	0.803 ± 0.032	-0.71	-1.24	-0.51
5.5	0.681 ± 0.070	0.777 ± 0.091	0.796 ± 0.032	-0.84	-1.49	-0.57
6	0.667 ± 0.071	0.769 ± 0.093	0.784 ± 0.031	-0.87	-1.51	-0.46
6.5	0.663 ± 0.076	0.763 ± 0.094	0.780 ± 0.031	-0.83	-1.43	-0.52
7	0.673 ± 0.088	0.757 ± 0.095	0.776 ± 0.031	-0.65	-1.10	-0.58
7.5	0.699 ± 0.106	0.752 ± 0.096	0.772 ± 0.031	-0.37	-0.66	-0.61
8	0.745 ± 0.132	0.749 ± 0.097	0.766 ± 0.030	-0.02	-0.16	-0.53

Z critical value at the level $\alpha = 5\%$ is equal to 2. Standard uncertainties are calculated in the appendix and are expressed for $k = 1$.

^aExperimental self-attenuation factor.

^bTheoretical self-attenuation factor.

^cMonte Carlo self-attenuation factor.

Table 3
Z score test results for experimental and Monte Carlo self-attenuation corrected activities and ²¹⁰Po activities

Sample	A_{ex}^a	A_{mc}^b	A_{po}^c	$Z_i (A_{ex}/A_{po})$	$Z_i (A_{ex}/A_{mc})$	$Z_i (A_{mc}/A_{po})$
1	81.4±16.3	88.3±9.1	81.1±3.9	0.02	-0.37	0.73
2	60.4±13.4	65.6±9.2	59.1±2.2	0.10	-0.32	0.69
3	23.6±9.9	25.6±9.8	35.3±1.0	-1.18	-0.14	-0.98
4	18.2±7.3	19.6±7.1	19.0±0.6	-0.11	-0.14	0.08
5	14.0±8.7	15.1±9.1	19.6±0.9	-0.64	-0.09	-0.49
6	79.3±16.9	90.7±11.3	86.5±2.2	-0.42	-0.56	0.36
7	144.0±30.3	159.3±19.3	150.7±6.3	-0.22	-0.43	0.42
8	120.5±24.1	139.7±14.0	115.3±4.8	0.21	-0.69	1.65
9	41.2±15.9	56.1±19.4	45.1±1.8	-0.24	-0.59	0.56
10	250.2±46.6	-	221.6±9.8	0.60	-	-
11	65.5±16.1	80.5±14.0	78.8±3.1	-0.81	-0.70	0.12
12	98.5±25.1	106.8±22.1	98.5±9.1	0.00	-0.25	0.35
13	124.1±24.3	145.0±13.4	150.5±4.4	-1.07	-0.75	-0.39
14	64.2±13.4	84.4±10.1	72.5±2.2	-0.61	-1.20	1.15
15	59.1±12.6	72.0±9.1	55.4±1.9	0.29	-0.83	1.79
16	50.8±14.4	61.9±13.9	41.7±1.3	0.63	-0.55	1.45
17	98.6±23.8	112.4±19.0	104.7±3.3	-0.25	-0.45	0.40
18	42.2±15.1	52.1±16.3	39.0±2.5	0.21	-0.45	0.79
19	21.4±8.4	28.0±9.8	25.0±1.6	-0.42	-0.51	0.30
20	109.3±22.7	143.2±15.5	110.2±4.4	-0.04	-1.21	1.93

Standard uncertainties are expressed for $k = 1$.

^aExperimental corrected ²¹⁰Pb activity (Bq/kg).

^bMonte Carlo corrected ²¹⁰Pb activity (Bq/kg).

^c²¹⁰Po activity (Bq/kg).

Table 4
 χ^2 -test between experimental and Monte Carlo self-attenuation corrected activities and ²¹⁰Po activities.

Activity (Bq/kg)	n	χ^2	P (%)	H_0 rejected
A_{ex} A_{po}	20	5.4	99.9	no
A_{ex} A_{mc}	19	10.4	99.4	no
A_{mc} A_{po}	19	16.9	59.6	no

n is the number of analysed soil samples ($\alpha = 5\%$).

closely ²¹⁰Pb corrected activities agree with ²¹⁰Po measurements. Thus results of ²¹⁰Po validate ²¹⁰Pb self-attenuation corrections and prove the successful efficiency calibration of the 46.5 keV line. The fact that we applied the experimental self-attenuation correction found for the IRSN reference material to 20 soil samples stems from the fact that their density and mass attenuation coefficient are almost identical, taking into account the practical difficulty to determine directly self-attenuation correction for each investigated sample. This is only valid for environmental solid samples, whose density ranges between 0.8 and 1.4 g/cm³ and whose mass attenuation coefficient ρ is around 0.4 cm²/g, which is the case in the majority of soil samples.

6. Conclusion

In this work, for a good measurement of ²¹⁰Pb by gamma spectrometry we have calibrated the HPGe detector for the 46.5 keV line. Experimental, theoretical and Monte Carlo self-attenuation corrections were carried out and are in coherence. An alpha spectrometry procedure for ²¹⁰Po was

developed, firstly to verify efficiency calibration and self-attenuation correction for ²¹⁰Pb determination, and secondly to measure ²¹⁰Po in environmental solid samples. This procedure was validated by some reference materials. The overall yield obtained is 80% by using microwave digestion under pressure, which appears efficient in the mineralization of samples for ²¹⁰Po determination. The good agreement obtained with the ²¹⁰Pb results and ²¹⁰Po determination validates different self-attenuation corrections and efficiency calibration for ²¹⁰Pb. The results clearly show a good Monte Carlo simulation of our HPGe detector.

Our proposed method for using experimental self-attenuation correction of reference sample (IRSN 77 SR 300) is valid for environmental solid samples whose density ranges between 0.8 and 1.4 g/cm³ and whose mass attenuation coefficient is around 0.4 cm²/g. On the other hand, an alternative method consists of using many reference solid samples to generalise self-attenuation correction, depending on density and mass attenuation coefficient. Unfortunately, this method will be expensive and time consuming.

Finally ²¹⁰Po alpha spectrometry procedure is also valid for foodstuffs whose quantity of dry sample to analyse was fixed to 5 g.

Acknowledgments

We thank the Swiss Federal Commission for Scholarships for Foreign Students for grants, Philippe Spring for radioactivity source deposition, J.C. Lavanchy for assistance in the determination of the chemical composition of the samples, M. Ngachin and M. Ngoko Djiokap for

sampling. ICTP (through the OEA-AC-71) is thanked for supporting one of the co-authors (MKN).

Appendix. Self-attenuation correction uncertainty calculations

Experimental self-attenuation correction

Efficiency of HPGe detector for IRSN solid reference sample (ε_s) and liquid calibration sample (ε_r) is

$$\left(\frac{u_{f_{\text{ex}}}}{f_{\text{ex}}}\right)_2^2 = \left[\begin{array}{l} \frac{a_0^2}{f^2} \left(\frac{u_{a_0}}{a_0}\right)^2 + \frac{h^2 a_1^2}{f^2} \left(\frac{u_{a_1}}{a_1}\right)^2 + b_0^2 \left(\frac{u_{b_0}}{b_0}\right)^2 + h^2 b_1^2 \left(\frac{u_{b_1}}{b_1}\right)^2 + h^4 b_2^2 \left(\frac{u_{b_2}}{b_2}\right)^2 \\ + h^2 \left[\frac{a_1 + 2a_2 h}{f} - (b_1 + 2b_2 h) \right] \left(\frac{u_h}{h}\right)^2 + 2 \left[\begin{array}{l} \frac{h}{f^2} u(a_0, a_2) + \frac{h^2}{f^2} u(a_0, a_2) + \frac{h^3}{f^2} u(a_1, a_2) \\ + hu(b_0, b_1) + h^2 u(b_0, b_2) + h^3 u(b_1, b_2) \end{array} \right] \end{array} \right] \left(\frac{1}{b_0 + b_1 h + b_2 h^2}\right)^2, \quad (\text{A.7})$$

given by

$$\varepsilon_{r,s} = \frac{N_{r,s}}{A_{r,s} m_{r,s} p} \quad (\text{A.1})$$

where $N_{r,s}$, $A_{r,s}$ and $m_{r,s}$ are, respectively total count rates, activities and mass of the solid reference sample and liquid calibration sample and p is the emission probability of the 46.5 keV line.

Thus experimental self-attenuation factor will be calculated by

$$f_{\text{ex}} = \frac{\varepsilon_s}{\varepsilon_r} = \frac{N_s}{A_s m_s} \frac{A_r m_r}{N_r}. \quad (\text{A.2})$$

Knowing that the mass of our cylindrical samples may be written as

$$m_{r,s} = \pi r^2 h \rho_{r,s} \quad (\text{A.3})$$

Eq. (A.2) becomes

$$f_{\text{ex}} = \frac{N_s}{A_s \rho_s} \frac{A_r \rho_r}{N_r} \quad (\text{A.4})$$

where $\rho_{r,s}$ are densities of the solid reference and liquid calibration samples, and its standard uncertainty is written as

$$\left(\frac{u_{f_{\text{ex}}}}{f_{\text{ex}}}\right)_1^2 = \left(\frac{u_{N_s}}{N_s}\right)^2 + \left(\frac{u_{A_s}}{A_s}\right)^2 + \left(\frac{u_{\rho_s}}{\rho_s}\right)^2 + \left(\frac{u_{N_r}}{N_r}\right)^2 + \left(\frac{u_{A_r}}{A_r}\right)^2 + \left(\frac{u_{\rho_r}}{\rho_r}\right)^2. \quad (\text{A.5})$$

The experimental self-attenuation factor is also given approximately by:

$$f_{\text{ex}}(h) = \frac{\varepsilon_s}{\varepsilon_r} = \frac{a_0 + a_1 h + a_2 h^2}{b_0 + b_1 h + b_2 h^2} \quad (\text{A.6})$$

and its fitting uncertainty is calculated by the square root of the variance of the fitted $f_{\text{ex}}(h)$:

$$\left(\frac{u_{f_{\text{ex}}}}{f_{\text{ex}}}\right)_2^2 = \frac{1}{f_{\text{ex}}^2} \left(\begin{array}{l} \left(\frac{\partial f}{\partial a_0}\right)^2 u_{a_0}^2 + \left(\frac{\partial f}{\partial a_1}\right)^2 u_{a_1}^2 + \left(\frac{\partial f}{\partial a_2}\right)^2 u_{a_2}^2 + \left(\frac{\partial f}{\partial b_0}\right)^2 u_{b_0}^2 \\ + \left(\frac{\partial f}{\partial b_1}\right)^2 u_{b_1}^2 + \left(\frac{\partial f}{\partial b_2}\right)^2 u_{b_2}^2 + \left(\frac{\partial f}{\partial h}\right)^2 u_h^2 \end{array} \right) + \frac{2}{f_{\text{ex}}^2} \left[\begin{array}{l} \frac{\partial f}{\partial a_0} \frac{\partial f}{\partial a_1} u(a_0, a_1) + \frac{\partial f}{\partial a_0} \frac{\partial f}{\partial a_2} u(a_0, a_2) + \frac{\partial f}{\partial a_1} \frac{\partial f}{\partial a_2} u(a_1, a_2) \\ + \frac{\partial f}{\partial b_0} \frac{\partial f}{\partial b_1} u(b_0, b_1) + \frac{\partial f}{\partial b_0} \frac{\partial f}{\partial b_2} u(b_0, b_2) + \frac{\partial f}{\partial b_1} \frac{\partial f}{\partial b_2} u(b_1, b_2) \end{array} \right].$$

This leads to the following simple and convenient form:

where u_i is the standard uncertainty of the i th parameter and $u(i, j)$ is the covariance between parameters i and j .

Finally, the standard uncertainty of $f_{\text{ex}}(h)$ is given by the square root of the following expression:

$$\left(\frac{u_{f_{\text{ex}}}}{f_{\text{ex}}}\right)^2 = \left(\frac{u_{f_{\text{ex}}}}{f_{\text{ex}}}\right)_1^2 + \left(\frac{u_{f_{\text{ex}}}}{f_{\text{ex}}}\right)_2^2. \quad (\text{A.8})$$

Theoretical self-attenuation correction

The theoretical calculation of the self-attenuation factor and its uncertainty are performed, respectively, by

$$f_{\text{th}}(h) = \left(\frac{\lambda + \mu_r \rho_r}{\lambda + \mu_s \rho_s}\right) \left(\frac{1 - e^{-(\lambda + \mu_s \rho_s)h}}{1 - e^{-(\lambda + \mu_r \rho_r)h}}\right) \quad (\text{A.9})$$

$$\left(\frac{u_{f_{\text{th}}}}{f_{\text{th}}}\right)^2 = \frac{1}{f_{\text{th}}^2} \left[\left(\frac{\partial f_{\text{th}}}{\partial \lambda}\right)^2 u_{\lambda}^2 + \left(\frac{\partial f_{\text{th}}}{\partial \mu_r}\right)^2 u_{\mu_r}^2 + \left(\frac{\partial f_{\text{th}}}{\partial \mu_s}\right)^2 u_{\mu_s}^2 + \left(\frac{\partial f_{\text{th}}}{\partial \rho_r}\right)^2 u_{\rho_r}^2 + \left(\frac{\partial f_{\text{th}}}{\partial \rho_s}\right)^2 u_{\rho_s}^2 + \left(\frac{\partial f_{\text{th}}}{\partial h}\right)^2 u_h^2 \right] \quad (\text{A.10})$$

where the u_i are standard uncertainties for the i parameters.

References

- [1] N. Hussain, G. Kim, T.M. Church, W. Carey, Appl. Radiat. Isot. 47 (1996) 473.
- [2] T. Pilleyre, S. Sanzelle, D. Miallier, J. Faïn, F. Courtine, Radiat. Meas. 41 (2006) 323.
- [3] G. Jia, M. Belli, M. Blasi, A. Marchetti, S. Rosamilia, U. Sansone, J. Radioanal. Nucl. Chem. 247 (2001) 491.
- [4] G. Jia, G. Torri, Appl. Radiat. Isot. 65 (2007) 1.
- [5] K. Debertin, R.G. Helmer, Gamma and X-ray Spectrometry with Semiconductor Detectors, Elsevier, Amsterdam, 1988.
- [6] E.G. San Miguel, J.P. Pérez-Moreno, J.P. Bolivar, R. Garcia-Tenorio, J.E. Martin, Nucl. Instr. and Meth. A 493 (2002) 111.
- [7] J.A. Sanchez-Cabeza, P. Masqué, I. Ani-Ragolta, J. Radioanal. Nucl. Chem. 227 (1–2) (1998) 19.
- [8] T. Miura, K. Hayano, K. Nakayama, Anal. Sci. 15 (1999).
- [9] N. Vajda, J. LaRosa, R. Zeisler, P. Danesi, G. Kis-Benedek, J. Environ. Radioactivity 37 (3) (1997) 355.

- [10] P. Gehnes, V. Thoste, 1981, Prospection d'uranium au Nord-Cameroun, rapport non diffusé, Hannover.
- [11] M. Oesterlen, 1985, Uranium Exploration in North Cameroon, unpublished report, Hannover.
- [12] J.P. Pérez-Moreno, E.G. San Miguel, J.P. Bolivar, J.L. Aguado, Nucl. Instr. and Meth. A 491 (2002) 152.
- [13] IRSN, Résultats de l'intercomparaison 77 SR 300, Mesure de la radioactivité naturelle dans un sédiment de lac, Rapport DEI/STEME-2005-07, Le Vésinet, France.
- [14] IEC/TC 45, International Electrotechnical Commission, Calibration and use of Germanium spectrometers for the measurement of gamma-ray emission rates of radionuclides, Geneva.
- [15] Detector Description and Simulation Tool CERN Program Library Long Writeup W5013, <http://wwwasdoc.web.cern.ch/wwwasdoc/geant_html3/geantall.html>.
- [16] J.-P. Laedermann, J.-F. Valley, S. Bulling, F.O. Bochud, Med. Phys. 31 (2004) 1614.
- [17] J.-P. Laedermann, M. Décombaz, Appl. Radiat. Isot. 52 (2000) 419.
- [18] M. Garcia-Talavera, H. Neder, M.J. Daza, B. Quintana, Appl. Radiat. Isot. 52 (2000) 777.
- [19] F. Bochud, C.J. Bailat, T. Buchillier, F. Byrde, E. Schmid, J.-P. Laedermann, Nucl. Instr. and Meth. A 569 (2006) 790.
- [20] J.J. Gostely, J.-P. Laedermann, Appl. Radiat. and Isot. 52 (2000) 447.
- [21] P. Vesterbacka, T.K. Ikäheimonen, Anal. Chim. Acta 545 (2005) 252.
- [22] SAIDOU, F. Bochud, J.-P. Laedermann, M.G. Kwato Njock, P. Froidevaux, Appl. Radiat. Isot., submitted.